Incoherent tune measurement of an ion storage ring using single ions

T. Liao,[1,2] C. Guo,[1,2] X. L. Yan,[1,*] X. Zhou,[1,2,†] Y. M. Xing,[1,‡] M. Wang,[1,2] Y. J. Yuan,[1,2,§] Y. H. Zhang,[1,2] X. H. Zhou,[1,2] M. Zhang,[1,2] W. W. Ge,[1] H. Y. Jiao,[1,2] Y. L. Jiang,[3] L. J. Mao,[1] R. J. Chen,[1,4] C. Y. Fu,[1] R. S. Mao,[1] J. C. Yang,[1] S. A. Litvinov,[4] and Yu. A. Litvinov[4]

[1]*CAS Key Laboratory of High Precision Nuclear Spectroscopy, Institute of Modern Physics, Chinese Academy of Sciences, Lanzhou 730000, China*

[2]*School of Nuclear Science and Technology, University of Chinese Academy of Sciences, Beijing 100049, China*

[3]*Lanzhou University, No. 222 South Tianshui Road, Lanzhou 730000, China*

[4]*GSI Helmholtzzentrum für Schwerionenforschung, Planckstraße 1, 64291 Darmstadt, Germany*

(Received 21 March 2023; revised 20 January 2024; accepted 15 April 2024; published 4 June 2024)

The measurement of betatron tunes is important in the studies of beam dynamics in circular accelerators. Here, we report a new method to extract the fractional tune values using revolution times of single ions stored for a few hundred turns in a heavy-ion storage ring utilizing a single time-of-flight detector. The experiment was done at the experimental Cooler Storage Ring (CSRe) in Lanzhou. The unbunched cocktail secondary beam was injected into the ring and allowed to coast without further excitation. Since the average number of simultaneously stored ions inside the 128.8 m-circumference ring was merely ~20, the obtained tune values are considered to be incoherent. Given that the revolution time of an individual ion is related to its momentum, the chromaticity of the ring could be addressed. Moreover, the data indicate a possible beam mismatch in vertical direction $\hat{y}$ at the injection into CSRe. The new method is developed for ultralow beam intensities and is thus a sensitive approach to tune measurements. Thanks to its simplicity, the method can straightforwardly be employed at other circular accelerators by applying the same detection approach.

DOI: 10.1103/PhysRevAccelBeams.27.062801

I. INTRODUCTION

In a storage ring, a stored particle travels on a spiral trajectory around the closed reference orbit. Separated into two orthogonal coordinates in the transverse plane, this motion is characterized by the corresponding betatron oscillations in $\hat{x}$ (horizontal) and $\hat{y}$ (vertical) directions. The betatron tune in each direction is a characteristic parameter of the machine, representing the number of betatron oscillations within one revolution [1]. For a very low-intensity beam containing only a few ions, the intrabeam and beam-environment interactions can be neglected, and the corresponding tunes, i.e., the incoherent tunes, are solely determined by the machine lattice settings. According to the theory of resonance driving terms RDT_{jklm} [2,3], the machine design should avoid the single-ion resonance condition:

$$(j-k)Q_x + (l-m)Q_y = r, \tag{1}$$

where j, k, l, m, and r are non-negative integers, Q_x and Q_y are the tune values in transverse orthogonal directions $\hat{x}$ and $\hat{y}$, respectively. The sum $j+k+l+m$ is called the order of the resonance. If the tunes satisfy the condition (1), resonances may appear and cause beam loss. In this context, precision measurement and feedback control of the incoherent tune values are essential in the design, commission, and operation of circular accelerators.

Usually the measurement of betatron tunes is focused on the fractional part of the tunes, which can be found by detection of the beam position oscillations using a beam position monitor (BPM) at any single location of the machine [4]. The integer part is usually calculated by an ion-optical code or can also be measured when the number of BPMs distributed along the ring is greater than $2Q$ [5].

In conventional tune measurement procedures, one relies on a coherent beam excitation and subsequent measurement of the driven oscillation. In these measurements, turn-by-turn transverse beam positions and/or side bands of beam revolution frequency harmonics are obtained using nondestructive devices such as beam position monitors [5] and/or Schottky [6] detectors. However, these monitors are often not sensitive enough, so high-intensity and/or bunched beams are required to guarantee a sufficient

*yanxinliang08@impcas.ac.cn
†zhouxu@impcas.ac.cn
‡xym@impcas.ac.cn
§yuanyj@impcas.ac.cn

signal-to-noise ratio. At the same time, the repulsive intrabeam Coulomb force between charged ions weakens the focusing force, leading to shifts of betatron tunes in the two transverse directions. High beam intensity may stimulate beam impedance and collective effects, further contributing to tune shift. The modification of the tunes due to beam intensity is referred to as coherent tune shift. Thus, it is challenging to measure incoherent tunes using the conventional methods, especially for compact size storage rings due to opposite requirements of high beam intensity and minimal space charge effects [7].

This work reports a new method developed at the heavy-ion storage ring in Lanzhou [8] to measure incoherent tunes via observing the revolution time oscillations instead of position oscillations of each stored ion. For ions with nonzero emittance, betatron oscillation leads to orbital length oscillation [9] and transverse position oscillation both of which naturally result in the detected revolution time oscillation. In the experiment, a time-of-flight (TOF) detector [10] is used to determine turn-by-turn revolution times of individual stored ions, which are then processed to determine the quantities of interest. The new method is single-ion sensitive, fast and suitable for ultralow beam intensity. The effects of the nonisochronous time response of the TOF detector as well as high-order magnetic fields in the ring are studied to explain the observed extra frequency components with abnormally large amplitudes in the measured revolution time oscillations. The chromaticity reflecting the dependence of the tune values on the ion momenta is addressed as well. Moreover, the amplitudes and initial phases of the tune components of ion trajectory can be obtained, which enables us to study the injection conditions of the storage ring.

The proposed measurement techniques utilizing TOF detectors do not require any extra beam excitation, as a single-particle sensitivity of the detectors at each turn enables investigation of individual ions with varying emittance. This method enables the acquisition of information about the emittance of stored ions and the incoherent tune of the circular machine using ultralow intensity beams, while also simplifying the machine operation scheme.

II. EXPERIMENT AND EXTRACTION OF TUNE VALUES

The experiment was done at the experimental Cooler Storage Ring (CSRe) in Lanzhou, China [8], mainly aiming at mass measurements of short-lived nuclides utilizing the isochronous mass spectrometry (IMS) [11–17]. The layout of the experimental facilities is presented in Fig. 1. The circumference of CSRe is about 128.8 m. The magnetic rigidity $B\rho$ of CSRe was set to 5.344 Tm. The transition energy γ_t factor of CSRe was set to 1.302. The theoretical betatron functions β_x and β_y and dispersion functions D_x and D_y along the reference closed orbit, s, in CSRe are

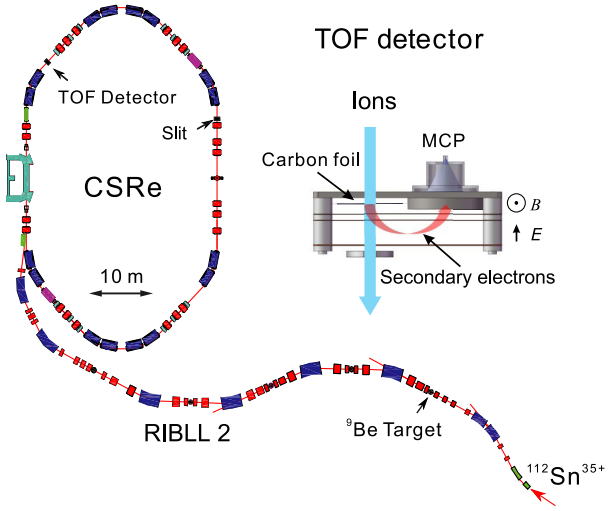

FIG. 1. Layout of the facilities used in the present experiment [11]. Various secondary ions produced in projectile fragmentation reaction of $^{112}Sn^{35+}$ beam were injected and stored in CSRe. The time-of-flight (TOF) detector with its major components is shown schematically in the inset. The dipole, quadrupole, and sextupole magnets are represented by blue, red, and green rectangles, respectively.

shown in Fig. 2. They were calculated with winAGILE code assuming linear lattice settings [18].

In the experiment, various secondary ions produced through projectile fragmentation of ^{112}Sn beams on a ^{9}Be target were injected into CSRe every 25 s. The radio frequency (rf) cavities in the CSRe were off by default. The stored ions are coasting in the ring until they are eventually lost. A TOF detector equipped with a thin carbon foil (thickness $\sim$19 $\mu g/cm^2$, or $\sim$90 nm, $\phi = 40$ mm) was

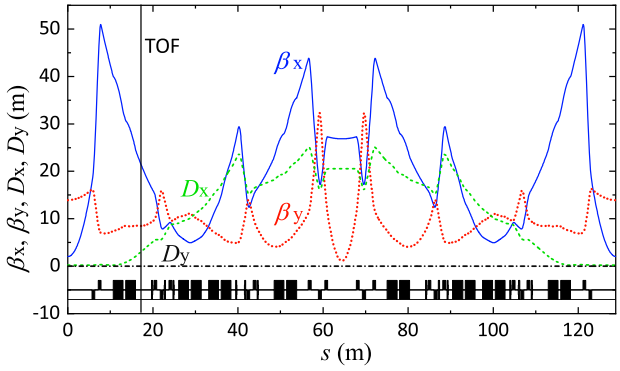

FIG. 2. Calculated twiss parameters of CSRe: horizontal $\beta_x(s)$ (blue solid line), vertical $\beta_y(s)$ (red dotted line) functions and horizontal $D_x(s)$ (green dashed line), vertical $D_y(s)$ (black dashed-dotted line) dispersion functions. Calculations were done with winAGILE code considering only linear lattice with only dipole and quadrupole magnetic fields [18]. The clamped "Rogowski" fringing field with FINT = 0.4 is used in this calculation. The position of the TOF detector is marked by the black solid vertical line.

installed inside the aperture of the ring [19–21], as shown in the inset of Fig. 1. The energy loss mechanism introduced by the TOF detector facilitates the study of turn-by-turn beam dynamics. Additionally, by utilizing all ions accumulated over thousands of injections, the characteristics of the beam within the full acceptance of the ring can be investigated.

The detection of the ions in the TOF detector is destructive. As a stored ion passed through the TOF detector at each turn, secondary electrons were released from the surface of the carbon foil [22] and guided to a set of microchannel plates (MCPs) [23] by the perpendicularly arranged electric and magnetic fields. The signals from the MCP were recorded using a digital oscilloscope for 200 μs after each injection, corresponding to about 300 revolution periods for different ion species with various mass-to-charge (m/q) ratios in CSRe acceptance. From the recorded signals, the sequences of passing times as a function of revolution number were obtained. The detection efficiency at each ion passage ranges from 10% to 90% depending on atomic number of the ions [19]. A 50-mm-wide slit in x direction was installed in the dispersive straight section of CSRe [24], as shown in Fig. 1, reducing the relative magnetic rigidity acceptance $\Delta B\rho/B\rho$ from approximately $\pm 1.7‰$ [10] to $\pm 0.4‰$ [25]. The slit was introduced to improve the mass measurement precision and is not required for tune measurement study. Throughout the experiment, a total of 13 805 injections were recorded, with an average of 20 stored ions per injection. Due to different mass-to-charge ratios of the stored ions, revolution times in CSRe differ among different ion species. The sequences of periodic timing signals, detected by the TOF detector and corresponding to different ions injected within a 500-ns injection-time window, were distinctly identified and assigned to their respective ions in the data analysis. For more details, see Refs. [11–13,25].

In the following, we choose a $^{72}Br^{35+}$ ion as a test case to describe the data analysis procedures. This ion is one of the 19 heavy ions stored simultaneously in the CSRe after injection. The obtained passing time sequence of this example ion is shown in Fig. 3. Such sequences are routinely analyzed in the mass measurement campaigns [26,27]. At first, accounting for energy losses in the thin carbon foil, a second-order polynomial fit function was used

$$t_{\mathrm{fit}}(N) = \sum_{i=0}^{2} a_i N^i = a_0 + a_1 N + a_2 N^2, \qquad (2)$$

where a_0, a_1, and a_2 are free parameters, and N is the number of revolutions. Here, a_0 represents the arriving time of the ion, $a_1 = \partial t/\partial N|_{N=0}$ the initial revolution time at the beginning of the measurement (zeroth turn) and $a_2 = 0.5 \cdot \partial^2 t/\partial N^2$ the half of the revolution time variation per turn caused by the energy loss of ions penetrating the TOF detector [28]. The fit residuals to the data in Fig. 3 are presented in Fig. 4(a), the distribution of which has a standard deviation of 56.5 ps.

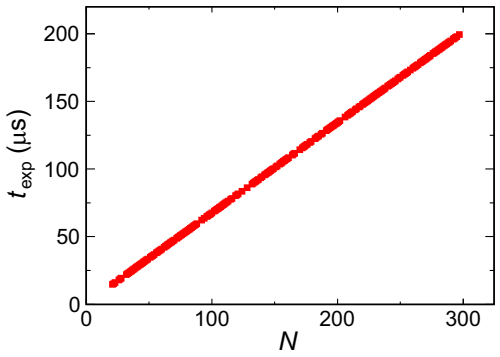

FIG. 3. Measured passing times t_{exp} as a function of the revolution number N of the example single $^{72}Br^{35+}$ ion.

To search for possible periodic features hidden in the fit residuals, a modified digital Fourier transform (DFT) [29] was applied

$$\mathrm{Amp}(f) = \frac{2}{n_s}\left\{\left[\sum_{j=1}^{n_s} X_{N_j}(2\pi f N_j)\right]^2 + \left[\sum_{j=1}^{n_s} X_{N_j}\sin(2\pi f N_j)\right]^2\right\}^{0.5}, \qquad (3)$$

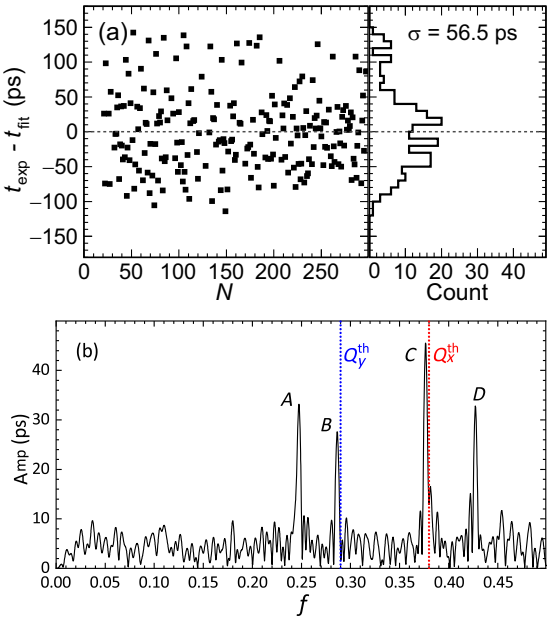

FIG. 4. (a) Left: residuals of the second-order polynomial fit to the data illustrated in Fig. 3. Right: the corresponding projection histogram. (b) The Fourier transform of the data in panel (a). The theoretical fractional tune value in $\hat{x}$ ($\hat{y}$) direction calculated using the linear lattice setting as shown in Fig. 2 is 0.38 (0.29) and is indicated by red (blue) doted line at the corresponding frequency location.

where n_s is the total number of timestamps measured, $X_{N_j} = t_{\mathrm{exp}}(N_j) - t_{\mathrm{fit}}(N_j)$ is the fit residual at the revolution number N_j, and f is the oscillation frequency. Because the X_{N_j} sequence is sampled once per revolution, the DFT analysis can only detect periodic components within frequency range from 0 to 0.5 according to Nyquist-Shannon sampling theorem [30]. For a dataset X_{N_j} with infinite discrete data generated by a pure sinusoidal wave, $X_{N_j} = A\sin(2\pi\nu N_j + \phi)$, $\mathrm{Amp}(f)$ is a δ function within the effective frequency range from 0 to 0.5: $\mathrm{Amp}(f) = A$ when $f = \{\nu\}$ or $1 - \{\nu\}$, where $\{\nu\}$ is the fraction part of ν, otherwise $\mathrm{Amp}(f) = 0$. If X_{N_j} contains random errors or the data sample size was limited, background noise will rise in the $\mathrm{Amp}(f)$ spectrum.

The obtained $\mathrm{Amp}(f)$ spectrum for this single ion is shown in Fig. 4(b). Four significant peaks labeled with A, B, C, and D are found in the $0 \le \{f\} \le 0.5$ range. This means that four periodic components exist in the studied time sequence. The same analysis was applied to all recorded time sequences of all ions observed in the experiment. Similar pattern with four peaks was observed, indicating that this is a general feature for all ions.

To account for these four periodic components, the fit function (2) was modified to

$$\begin{aligned} t_{\mathrm{fit}}(N) = {} & a_0 + a_1 N + a_2 N^2 \\ & + A_A \sin\left[2\pi(b_{0A}N + b_{1A}N^2) + \phi_A\right] \\ & + A_B \sin\left[2\pi(b_{0B}N + b_{1B}N^2) + \phi_B\right] \\ & + A_C \sin\left[2\pi(b_{0C}N + b_{1C}N^2) + \phi_C\right] \\ & + A_D \sin\left[2\pi(b_{0D}N + b_{1D}N^2) + \phi_D\right], \end{aligned} \tag{4}$$

where the quadratic terms are introduced due to the energy loss of particles in the foil of the TOF detector. Using this new function, the standard deviation of fit residuals is reduced from 56.5 to 27.1 ps, which is close to the intrinsic time resolution of about 20 ps of the TOF detector used in the experiment [20].

We interpret these periodic components as being due to betatron oscillations of the ion in the ring. Since only a few ions inside the 128.8 m CSRe ring were stored simultaneously, the motion of each ion is not influenced by other ions. Hence, the measured frequencies are considered as *incoherent*. In the sinelike terms, A_i and ϕ_i (i runs over A, B, C, and D) represent amplitudes and initial phases of the measured revolution time oscillation. The first derivative of each polynomial in phase terms

$$b_i = b_{0i} + 2b_{1i}N \tag{5}$$

is the phase advance per turn of the sine function. The b_i's are the fractional frequencies of betatron oscillations at each revolution number N [10]. It is worth noting that both the frequency b_i and phase $\psi_i = 2\pi(b_{0i}N + b_{1i}N^2) + \phi_i$ vary with turn number N, while the amplitude A remains constant throughout all N.

III. ORIGINS OF PERIODIC COMPONENTS

To find out possible origin of the four peaks observed in Fig. 4(b), simulations with MADX code [31] have been performed with the linear lattice shown in Fig. 2, and the calculated Q_x and Q_y are 1.620 and 2.710, respectively. A time sequence t of 300 turns has been simulated for an ion with $\varepsilon_x = 20\ \pi$ mm mrad and $\varepsilon_y = 20\ \pi$ mm mrad. The time resolution of ~20 ps of the TOF detector was considered. A similar DFT analysis using Eq. (3) was applied to the simulated data. The obtained $\mathrm{Amp}(f)$ spectrum is shown as a solid black line in Fig. 5(a). Since 100% detection efficiency was assumed in the simulated data, the resulting $\mathrm{Amp}(f)$ spectrum exhibits a lower noise compared to the experimental result shown in Fig. 4. As expected, with the linear lattice setting, only one sizeable peak with about 100 ps height is found at $f \sim 0.38$ below $f = 0.5$, which is exactly equal to the theoretical fractional Q_x of the linear lattice. The peak height at C, A_C, is equal to the amplitude of the orbit length oscillation δC divided by the velocity of the ion. Here, $\delta C = \sqrt{\varepsilon_x(\gamma_x D_x^2 + 2\alpha_x D_x D_x' + \beta_x D_x' D_x')}$, where ε_x is the emittance of the ion and $\alpha_x, \beta_x, \gamma_x, D_x$, and $D_x' = \partial D_x/\partial s$ are lattice parameters at the location of TOF [9] as shown in Fig. 2. As a result of zero D_y throughout the ring, the orbital length oscillation introduced by vertical betatron motion is negligible for the uncoupled linear lattice.

In the real world, various nonlinear (high-order) magnetic fields arising from undesirable magnet design defects [33] will cause coupling of motions in $\hat{x}$ and $\hat{y}$ directions. Sometimes, sextupole magnetic fields are specially introduced to correct chromaticity, transition energy γ_t curve [34] and dynamic aperture, etc. A sextupole field will result in a nonlinear betatron coupling, while a skew quadrupole field, for instance, will lead to a linear betatron coupling [1]. After adding normal sextupole and skew quadrupole fields to the uncoupled linear lattice, the resulting $\mathrm{Amp}(f)$ spectrum is shown by the red dotted line in Fig. 5(a). The position of the original peak at the fractional Q_x [peak C in Fig. 5(a)] is shifted, which is termed as *detuning* in Ref. [2]. Besides that, additional peaks noted A, B, and D appear at $f \sim 0.23$, 0.29, and 0.42, respectively. The frequencies of these extra peaks match well with the observed f_A, f_B, and f_D peaks in Fig. 4(b) but with much smaller amplitudes. In this simulation, an additional peak with frequency $f_B^{\mathrm{sim}} = Q_y^{\mathrm{sim}}$ is driven by the skew quadrupole fields and peaks with frequencies of $f_A^{\mathrm{sim}} = 1\text{–}2Q_x^{\mathrm{sim}}$ and $f_D^{\mathrm{sim}} = 1\text{–}2Q_y^{\mathrm{sim}}$ are driven by the normal sextupole fields. The heights of peaks $A(B)$ and $C(D)$ exhibit a clear correlation in the simulation. The amplitude ratios, A_A/A_C^2 and A_D/A_B^2, are determined by the coupling strength between the motions in $\hat{x}$ and $\hat{y}$ directions which is in turn determined by the

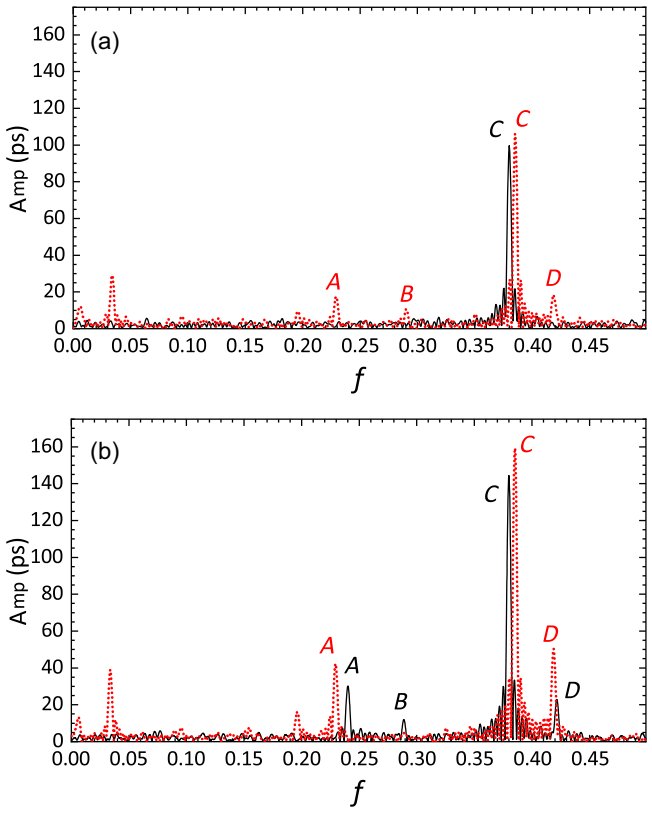

FIG. 5. DFT results of the simulated time sequence for an ion with $\varepsilon_x \sim 20\ \pi$ mm mrad and $\varepsilon_y \sim 20\ \pi$ mm mrad, using linear lattice (black solid line) and lattice with normal sextupole and skew quadrupole fields (red dotted line). The average flight times of secondary electrons t_e released at any position of carbon foil in detector are constant in (a). Using SIMION programs [32], the relationship between t_e and position x, y are calculated and considered in (b). See text for details.

added high-order magnetic fields in the ring lattice. Obviously, the simulated spectrum has several extra peaks at $f \sim 0.01$, 0.03, and 0.2, which are attributed to the coupling magnets and are not clearly presented due to high noise level in the experimental spectrum.

Besides orbital length oscillations, the position dependence of time responses of TOF detector can also drive periodic components in the measured time sequences of a stored ion with nonzero emittance. The passing position of the stored ion at the TOF detector is different from turn to turn and is oscillating with amplitude of $\sqrt{\varepsilon_{x,y}\beta_{x,y}}$. The measured passing time of the ion is the actual arrival time of the ion at the carbon foil of the detector plus the time of flight of the induced secondary electrons from carbon foil to the MCP (see inset in Fig. 1). Using SIMION program [32], the flight times of secondary electrons t_e from carbon foil to MCP were simulated for the TOF detector used in the experiment. It turned out that t_e is a second-order polynomial function of ion passage position (x, y) at carbon foil, see Appendix. After considering this position-dependent time response detector effect, Fig. 5(b) shows the new Amp(f) spectrum for the same simulated ion. Now, with the linear lattice (solid black line), the height of the peak C is increased to about 160 ps and additional three peaks appear at $f \sim 0.23$, 0.29, and 0.42 solely due to the detector effect. In this simulation, the oscillation observed in the recorded time sequences at frequency $f_C^{\rm sim} = Q_x^{\rm sim}$ is a combined result of the orbital length oscillation and detector effects arising from position oscillation in the $\hat{x}$-direction. The oscillation in the response-time of the TOF detector has an amplitude that is equal to $\partial t_e/\partial x\sqrt{\varepsilon_x\beta_x}$. Depending on the phase difference between the orbital length oscillation and response-time oscillation, the amplitude of the combined oscillation may either increase or decrease. This phase difference is determined by the location of the TOF detector in the ring. For the detector used in this experiment, the amplitude of the combined oscillation (at peak C) is increased with a positive $\partial t_e/\partial x$. The height of the additional peak with frequency $f_B^{\rm sim} = Q_y^{\rm sim}$ is equal to $A_B = \partial t_e/\partial y\sqrt{\varepsilon_y\beta_y}$. Similarly, the heights of the peaks with frequency $f_A^{\rm sim} = 1\text{–}2Q_x^{\rm sim}$ and $f_D^{\rm sim} = 1\text{–}2 \cdot Q_y^{\rm sim}$ are equal to $A_A = \partial^2 t_e/\partial x^2(\varepsilon_x\beta_x)/4$ and $A_D = \partial^2 t_e/\partial y^2(\varepsilon_y\beta_y)/4$, respectively. Therefore, the amplitudes of peak $A(B)$ and $C(D)$ exhibit clear relations: $A_A = m_1 A_C^2$ and $A_D = n_1 A_B^2$. Here m_1 parameter is determined by velocity of the ion and nonisochronous time response of the TOF detector, and n_1 parameter is solely determined by nonisochronous time response of the TOF detector. The dotted red line in Fig. 5(b) is the result with both detector effect and high-order fields added into the ring lattice. Compared to the solid black line, the resultant frequencies of all peaks are shifted. The peak B disappears due to the counter effects (by chance) of the different origins described above.

Unfortunately, the large height of extra peaks in spectrum in Fig. 4(b) could not completely be reproduced in the simulations, even by combining both effects from high-order fields and detector response as shown in Fig. 5(b) (see red dotted line). In the simulation, there are many free parameters that can affect the height of the DFT peaks, including allowed emittance of the ions, the time response profile of the TOF detector, and the high-order magnet fields settings of the ring lattice. Thus further investigations are needed to reproduce the heights of the four observed peaks in Fig. 4(b).

Figures 6(a) and 6(d) show the correlation between the experimental frequency values of b_A and b_C, b_D and b_B, respectively. Note that the frequencies are at the middle revolution number $N_{\rm mid}$ [the average turn number of the first and last measured time stamp in each time sequence $t(N)$] as defined in Eq. (4). This is due to the fact that the fitting error $\sigma(b_i)$ is minimized at this point [10]. If only ions with $\sigma(b_i) < 3.5 \times 10^{-4}$ (i runs over A, B, C, and D) are considered, the absolute value of Pearson correlation coefficient (PCC) [35] is 0.941 and 0.845, suggesting a strong correlation between these pairs of frequencies.

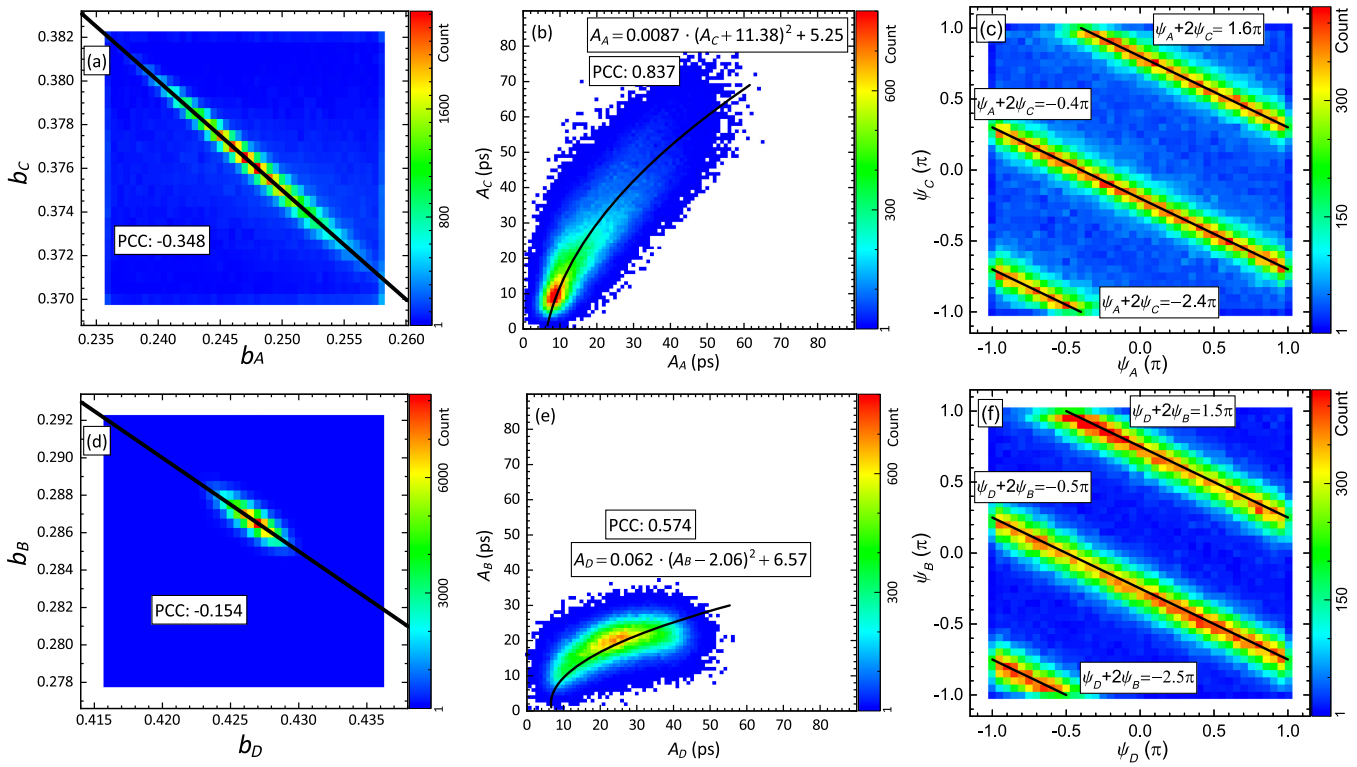

FIG. 6. Correlation between the frequency at middle revolution number N_{mid} b_A and b_C (a), b_D and b_B (d), the amplitudes A_A and A_C (b), A_D and A_B (e), the phases at middle revolution number N_{mid} ψ_A and ψ_C (c), ψ_D and ψ_B (f). The Pearson correlation coefficients (PCC) characterizing the correlation magnitude are shown where applicable. If only ions with $\sigma(b_i) < 3.5 \times 10^{-4}$ (i runs over A, B, C, and D) are considered, the number of scattering points in (a) and (b) will be significantly reduced, resulting in PCC values of -0.941 and -0.845 for (a) and (d), respectively. The solid black lines are drawn to guide the eye. The black solid lines in (a) and (d) illustrate equations $b_A + 2b_C = 1$ and $b_D + 2b_B = 1$, respectively.

As indicated by the black lines in Fig. 6, the relations can be well described using the linear function of $b_A + 2b_C = 1$ and $b_D + 2b_B = 1$, which is consistent with simulations shown in Fig. 5. Combining the correlation shown in Fig. 6 and simulations in Fig. 5, b_C (b_B) is assigned to be the fractional betatron tune in direction $\hat{x}$ Q_x ($\hat{y}$ Q_y).

Figure 6 displays correlations between peak heights A_A and A_C (b), A_D and A_B (e), and correlations between phase ψ_A and ψ_C (c), ψ_D and ψ_C (f) for all measured ions in the experiment. Here, as defined in Eq. (4), ψ is the phase at the middle revolution number N_{mid}: $\psi = 2\pi \cdot (b_0 N_{\mathrm{mid}} + b_1 N_{\mathrm{mid}}^2) + \phi$. It is evident from Fig. 6(b) that $A_C(A_B)$ follows a second-order polynomial function of $A_A(A_D)$, which satisfies the expectations of both RDT theory [2,3] and the simulated second-order position-dependent time response of the TOF detector. Besides that, a linear relations between ψ_A and ψ_C (ψ_D and ψ_B) are observed in Fig. 6(c) and 6(d). The value of $\psi_A + 2\psi_C$ and $\psi_D + 2\psi_B$ could be of interest in a correction scheme for the LHC [36]. The difference between phase values of $\psi_A + 2\psi_C = -0.4\pi \pm 2\pi$ and $\psi_D + 2\psi_B = -0.5\pi \pm 2\pi$ may indicate different origins of the corresponding oscillations.

In another experiment using the same single TOF detector, only two significant peaks in Amp(f) spectra were observed with secondary beam of $^{58}Ni^{19+}$ projectile fragments and $\gamma_t \sim 1.395$ setting of the ring [27,37,38]. No correlation was found between the two oscillating components. In a further experiment [10], also two uncorrelated peaks in the Amp(f) spectra were observed. In that work, two new TOF detectors in the so-called Bρ-defined IMS experiment [39,40] were employed and the transition γ_t of CSRe was set to 1.39. With the aid of ion-optical calculations, the two frequencies were assigned to the fractional tunes in $\hat{x}$ and $\hat{y}$ transverse directions, respectively. In still another experiment with a similar lattice of $\gamma_t \sim 1.302$ [41], four significant peaks appear at positions similar to those depicted in Fig. 4 of this paper. These observations indicate that the four peaks feature in the Amp(f) spectrum is a special characteristic of this ring lattice with $\gamma_t \sim 1.302$.

IV. DISCUSSION

In Sec. II, in the fitting of the time sequences by using Eq. (4), all the parameters were treated as free parameters. However, some of the parameters are not independent from each other as has been illustrated in Fig. 6. For example, b_A and b_C should satisfy $2b_C + b_A = 1$ and b_B and b_D satisfy $2b_B + b_D = 1$ at any revolution number N. This means

that, based on Eq. (5) and Fig. 6, the following restrictions apply:

$$\begin{aligned} 2b_{C0} + b_{A0} &= 1, \\ 2b_{B0} + b_{D0} &= 1, \\ 2b_{C1} + b_{A1} &= 0, \\ 2b_{B1} + b_{D1} &= 0. \end{aligned} \tag{6}$$

Using these constraints in the fitting process, b_i values with precision of 10^{-4} have been obtained (see, for example, Fig. 7) and are used in the following discussion. In fact, the emergence of additional induced oscillation components in the measured time sequences enhances the accuracy of the measured betatron tunes.

A. Chromaticity

The change of tunes due to the change of particle momentum is called chromaticity of a machine [4]. It can be defined as [42]

$$\xi = \frac{\Delta Q}{\Delta p/p}. \tag{7}$$

Typically, the natural chromaticity is large, indicating a large tune spread. A circulating beam with a large tune spread could encounter many resonances, and chromatic correction is needed to ensure good performance of a storage ring [1].

For the same ion species, the variation of momentum Δp and the corresponding variation of revolution time ΔT_{exp} (flight time per turn) are connected through the following relationship [15]:

$$\frac{\Delta T_{\mathrm{exp}}}{T_{\mathrm{exp}}} = \left(\frac{1}{\gamma_t^2} - \frac{1}{\gamma^2}\right)\frac{\Delta p}{p} = -\eta\frac{\Delta p}{p}. \tag{8}$$

Here, T_{exp} is the revolution time, which can be calculated as $T_{\mathrm{exp}} = a_1 + 2a_2 N$ with a_1 and a_2 being the fit parameters

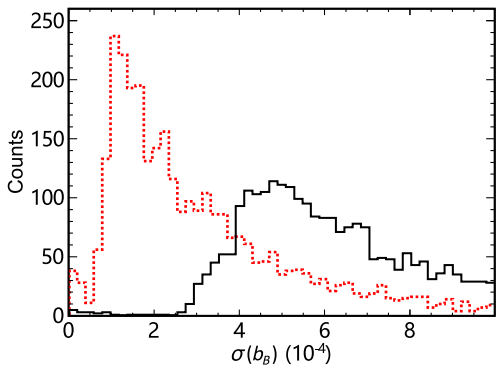

FIG. 7. Distribution of the fitting error of b_B, $\sigma(b_B)$, with (red line) and without (black line) the restriction of Eq. (6) in the fitting using Eq. (4).

in Eq. (4). $\eta = 1/\gamma^2 - 1/\gamma_t^2$ is the *phase-slip factor*. Combining Eqs. (8) and (7) gives

$$\xi = \frac{\Delta Q}{\Delta p/p} = -\eta\frac{\Delta Q}{\Delta T_{\mathrm{exp}}/T_{\mathrm{exp}}}. \tag{9}$$

Within the small momentum acceptance, limited by the slit in the ring [24], η can approximately be assumed to be constant. Furthermore, γ_t was set to 1.302 in this experiment and γ can be calculated from the ion velocity, which is approximated by the ratio of the mean orbit length $C = 128.8$ m and the measured revolution time T_{exp} [25]. Thus, the average chromaticity ξ can be derived from the relationship between the revolution times T_{exp} and the tunes b_i, i.e., the $b(T)$ curve or vice versa, the $b(T)$ correlation can be obtained assuming the theoretical chromaticity values.

In Fig. 8, examples of the $b(T)$ curves are shown for two different ion species with $\eta < 0$ and $\eta > 0$. Q and T determined at the middle revolution number N_{mid} are used. We note that the measured T_{exp} values used here have been corrected to eliminate the effects due to long-term magnetic field instabilities [25]. As the b_B (b_C) values depicted in Fig. 8 are the fractional parts of tunes measured at the middle revolution number N_{mid}, the real tunes in $\hat{y}$ ($\hat{x}$) direction should be $3 - b_B$ ($2 - b_C$) according to the WINAGILE calculations. The theoretical chromaticity values of ξ_x^{th} and ξ_y^{th} calculated from the linear lattice design (see Fig. 2) are -1.546 and -1.653, respectively. Using these theoretical values, the expected $b(T)$ relations are derived and shown as red lines in Fig. 8. For $\hat{y}$ direction, the theoretical $b(T)$ dependencies are not far off from the experimental $b_B(T)$ curves from which the fitted chromaticity are determined to be $\xi_y^{\mathrm{fit}} = -1.63 \pm 0.06$ ($^{49}Cr^{24+}$) and -1.93 ± 0.04 ($^{61}Cu^{29+}$), respectively. This indicates that the realistic incoherent tune and chromaticity values have been obtained for $\hat{y}$ direction. For $\hat{x}$ direction, it is difficult to derive ξ_x^{fit} from the experimental data as there is no obvious correlation between b_C and T_{exp} occurred in Figs. 8(a) and 8(b). The smaller absolute value of PCC in $\hat{x}$ direction, and the disagreements between ξ_x^{th} and ξ_x^{fit}, may due to chromaticity change caused by the high-order magnetic fields in the ring as discussed in Sec. III.

The method to extract chromaticity from measured time sequences has been developed in our previous work [10], where the velocity of every stored ion was measured directly employing two TOF detectors in a straight section of CSRe. Compared to single TOF detector scheme, the two TOF detectors scheme is superior for measuring the chromaticity of the ring [10]. In this paper, it is the first time that the chromaticity is addressed (although with large errors) using a single TOF detector. Furthermore, the correlations shown in Fig. 8 can be used to correct for the momentum dependence of the ion revolution times.

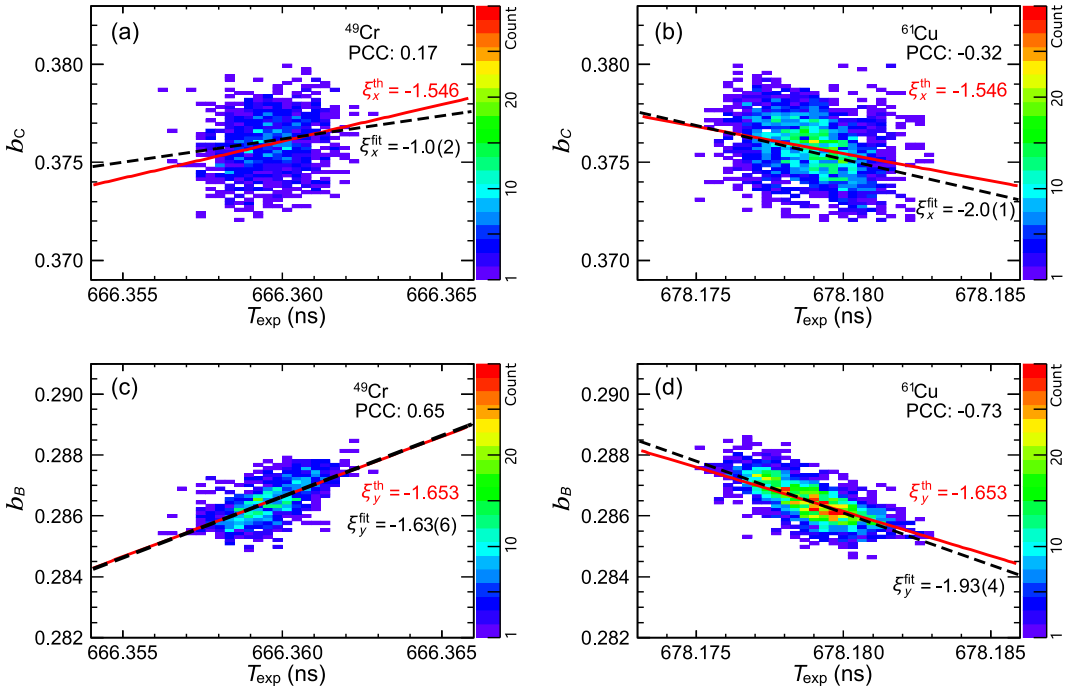

FIG. 8. Scatter plots of measured frequency b_C or b_B versus revolution times $T_{\rm exp}$ measured at the middle revolution number $N_{\rm mid}$ for $^{49}Cr^{24+}$ ($\eta < 0$) and $^{61}Cu^{29+}$ ($\eta > 0$) ions. Red solid lines display the expected $b(T)$ relations using the theoretical chromaticity values $\xi_x^{\rm th}$ or $\xi_y^{\rm th}$, which are calculated from the linear lattice design shown in Fig. 2. Black dashed line indicates the fitted chromaticity values $\xi_x^{\rm fit}$ or $\xi_y^{\rm fit}$. Only the ions with $\sigma(b_i) < 3.5 \times 10^{-4}$ [i could be C or B in Eq. (4)] are considered.

Therefore, it has an application potential to improve the resolving power of the storage ring mass spectrometry [14,15].

B. Injection into the ring

As discussed in Sec. III, the amplitudes of the periodic components $A_C(A_B)$ are proportional to the square root of emittance $\sqrt{\varepsilon_x}$ ($\sqrt{\varepsilon_y}$), and the phases $\psi_{C,B}$ are directly related to the phases of the corresponding betatron oscillations in $\hat{x}$ and $\hat{y}$ directions [10]. Figure 9 displays the scatter plots of A versus ψ at zeroth revolution number $N = 0$ in polar coordinates for the oscillations at frequency b_C and b_B for all ions across 13 805 injections. It is important to note that the value of ψ at the zeroth turn is not observed in the experimental data but rather is an extrapolation based on the fitting results using Eq. (4). It is evident in Fig. 9(b) that the scatterplot associated with b_B is asymmetric. Most of the ions are concentrated in the region $1.7\pi < \psi_y < 2.1\pi$ and 10 ps $< A_y <$ 30 ps. This observation indicates that a beam mismatch probably existed at the injection in $\hat{y}$ direction, which might lead to a reduction of the ring longitudinal and transverse acceptances [43]. However, due to the unknown contribution of the position dependence of the TOF time responses [20], a definitive conclusion whether this mismatch originates from position y or angle y' is not possible based only on this scatterplot. Dedicated measurements are needed to clarify this issue in

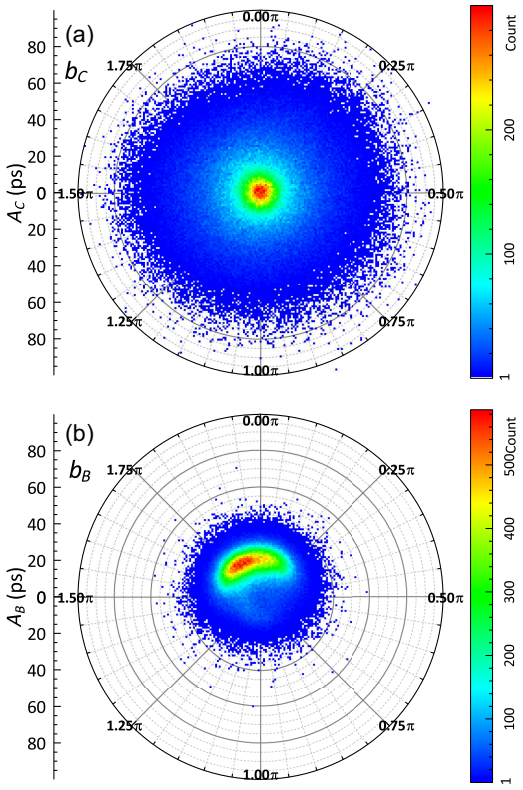

FIG. 9. Scatterplots of amplitudes A versus phases ψ at $N = 0$ for oscillation components with frequencies b_C (a) and b_B (b).

the future. In Fig. 9(b), some of the ions have much larger A_c values than the majority of the ions. From simulation results in Fig. 5, we know that one ion with $\varepsilon_x \sim 20\ \pi$ mm mrad will cause $A_C \sim 100$ps under the assumption of a linear lattice and a perfect isochronous time response of the TOF detector. The designed emittance acceptances of CSRe ring in isochronous mode are 20 π mm mrad in both $\hat{x}$ and $\hat{y}$ directions [8,44]. Therefore, it is a consistent explanation that the mismatch at the beam injection may reduce the acceptance of CSRe ring.

V. SUMMARY AND OUTLOOK

In this work, a fast, sensitive and high-resolution method for the "incoherent tune" measurement in the storage ring CSRe is reported. A single time-of-flight (TOF) detector was employed and only a few tens of ions from secondary cocktail beam were stored in the ring simultaneously. The incoherent tune values were extracted by explicitly considering the betatron oscillations in the fit function applied to the time sequences measured by the TOF detector for each ion, as a function of the revolution number. The overall measurement was completed 200 μs after each injection of the ions into the ring. In the experiment, both fractional betatron tune values and betatron oscillation phase at the injection in the $\hat{x}$ and $\hat{y}$ directions were measured. The assignment of the measured betatron tune values to Q_x and Q_y was accomplished with the assistance of ion-optical calculations. Correlated oscillation components in the measured revolution time of stored ions were observed in the specific $\gamma_t = 1.302$ lattice setting of CSRe. Higher order fields in the ring lattice and position dependence of TOF detector time responses are possible origins of this correlation. After taking this correlation into account in the data analysis, the measured tune values can be determined on an absolute precision level of 10^{-4}. Under reasonable conditions of time-respond profile of the TOF detector and high-order field profiles of the CSRe lattice, the absolute amplitudes of the oscillation components cannot be fully reproduced in the simulations. Additional studies, such as complementary tune measurement using beam position monitors (BPMs) and detailed measurement of the position-dependent time-response of the TOF detector, are necessary to address this issue in the future.

The tune versus revolution time $b(T)$ curves were utilized to address the chromaticity of CSRe by using all the stored ions in the experiment. The experimental $b(T)$ curves could be partly reproduced by the theoretical calculations assuming chromaticity values of the linear lattice setting, indicating that the incoherent tunes are plausibly obtained. Moreover, a nonsymmetric distribution of the amplitudes and phases of the periodic components at zeroth turn is observed. This indicates that a beam mismatch probably exists in $\hat{y}$ direction at the injection, which is likely to cause reduced longitudinal and transverse acceptances.

Traditional tune measurement methods often require additional rf equipment to bunch the relatively high intensity primary beam and a dedicated kicker system for beam excitation, in order to increase the oscillation of the beam centroid and enhance the signal-to-noise ratio. In contrast, this new method works with a cocktail secondary beams and boasts the main advantages of a single-ion sensitivity at each revolution turn, short measurement time for each ion, high precision with thousands of ions. As a result, incoherent tune measurements can be accomplished with tiny beam intensities without further beam excitation. This new method enables direct tune measurements with a single measurement and has the potential to enable fast beam optimizations at ultralow beam intensities.

For tasks of systematic machine studies, the new method can be an alternative or a complementary to the conventional tune-measurement methods utilizing electromagnetic probes, e.g., transverse Schottky detectors [45] and BPMs. Moreover, the chromaticity measurement method reported here has a potential application for improving the mass resolving power of the isochronous mass spectrometry with a single TOF detector [46]. Thanks to its simplicity, the new method can be straightforwardly adapted in other storage rings, such as the collector ring at FAIR [47,48] or Proton Synchrotron at CERN [49]. It can particularly be interesting for the experimental storage ring at GSI, where the installation of two TOF detectors is not feasible due to space limitation [50].

ACKNOWLEDGMENTS

This work is supported by the National Key R&D Program of China (Grant No. 2023YFA1606401), the Strategic Priority Research Program of Chinese Academy of Sciences (Grant No. XDB34000000), the NSFC (Grants No. 12305126, No. 12105333, No. 12135017, No. 12121005, No. 11905261, and No. 11905259). X. L. Y. acknowledge the support from the Young Scholar of Regional Development, CAS (Grant No. [2023]15). Y. M. X. acknowledge the support from the Youth Innovation Promotion Association of Chinese Academy of Sciences (Grant No. 2021419). R. J. C is supported by the International Postdoctoral Exchange Fellowship Program 2017 by the Office of China Postdoctoral Council (No. 60 Document of OCPC, 2017).

APPENDIX: SIMULATED TIME RESPONSE OF THE TOF DETECTOR

Using the SIMION software [32], the geometry structure and electromagnetic settings of the TOF detector were modeled for the TOF detector used in the experiment. The trajectories of the secondary electrons released from the surface of the carbon foil were simulated. The flight times of secondary electrons t_e from the carbon foil to MCP are depicted in Fig. 10. It turned out that t_e is a quadratic

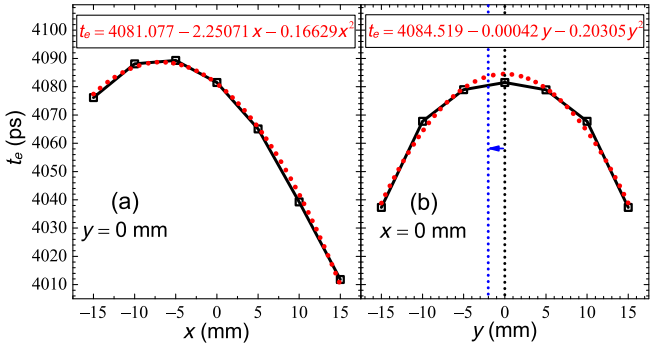

FIG. 10. Simulated flight times of secondary electrons t_e as a function of ion passage position (x, y) at the TOF detector (black square markers). The red dotted lines represent fitting results of the $t_e(x, 0)$ and $t_e(0, y)$ using second-order polynomial functions as shown in the black boxes. The simulated $t_e(0, y)$ is symmetric about $y = 0$. The center of the ion passing position in $\hat{y}$ direction is shifted to $y = -2$ mm to ensure an average nonzero $\partial t_e/\partial y$ value, see blue dotted lines.

polynomial function of the ion passage position (x, y), see the fitting function in this figure. Particularly, for theoretical calculations in Fig. 5, the average center position of the simulated ion orbit in direction $\hat{y}$ was shifted from the center of the carbon foil to -2 mm. This is done to ensure a nonzero average $\partial t_e/\partial y$ effect, otherwise, the additional peak labeled as B would not appear in the Amp(f) spectrum in Fig. 5(b).

[1] S.-Y. Lee, *Accelerator Physics*, 4th ed. (World Scientific Publishing Company, Singapore, 2018), https://doi.org/10.1142/9789813274686_0002.

[2] R. Bartolini and F. Schmidt, Normal form via tracking or beam data, Part. Accel. **59**, 93 (1998), https://cds.cern.ch/record/333077.

[3] A. Franchi, Studies and measurements of linear coupling and nonlinearities in hadron circular accelerators, Ph.D. thesis, beim Fachbereich Physik der Johann Wolfgang Goethe-Universität in Frankfurt am Main, 2006, https://publikationen.ub.uni-frankfurt.de/frontdoor/index/index/docId/2270.

[4] R. Jones, Measuring tune, chromaticity and coupling, arXiv:2005.02753.

[5] P. Zisopoulos, Y. Papaphilippou, and J. Laskar, Refined betatron tune measurements by mixing beam position data, Phys. Rev. Accel. Beams **22**, 071002 (2019).

[6] M. Betz, O. Jones, T. Lefevre, and M. Wendt, Bunched-beam Schottky monitoring in the LHC, Nucl. Instrum. Methods Phys. Res., Sect. A **874**, 113 (2017).

[7] K. Kojima, H. Okamoto, and Y. Tokashiki, Empirical condition of betatron resonances with space charge, Phys. Rev. Accel. Beams **22**, 074201 (2019).

[8] J. Xia, W. Zhan, B. Wei, Y. Yuan, M. Song, W. Zhang, X. Yang, P. Yuan, D. Gao, H. Zhao *et al.*, The heavy ion cooler-storage-ring project (HIRFL-CSR) at Lanzhou, Nucl. Instrum. Methods Phys. Res., Sect. A **488**, 11 (2002).

[9] Y. Shoji, Dependence of average path length betatron motion in a storage ring, Phys. Rev. ST Accel. Beams **8**, 094001 (2005).

[10] X. Zhou, M. Zhang, M. Wang, Y. H. Zhang, Y. J. Yuan, X. L. Yan, X. H. Zhou, H. S. Xu, X. C. Chen, Y. M. Xing *et al.*, In-ring velocity measurement for isochronous mass spectrometry, Phys. Rev. Accel. Beams **24**, 042802 (2021).

[11] Y. M. Xing, C. X. Yuan, M. Wang, Y. H. Zhang, X. H. Zhou, Y. A. Litvinov, K. Blaum, H. S. Xu, T. Bao, R. J. Chen *et al.*, Isochronous mass measurements of neutron-deficient nuclei from ^{112}Sn projectile fragmentation, Phys. Rev. C **107**, 014304 (2023).

[12] X. Xu, J. H. Liu, C. X. Yuan, Y. M. Xing, M. Wang, Y. H. Zhang, X. H. Zhou, Y. A. Litvinov, K. Blaum, R. J. Chen *et al.*, Masses of ground and isomeric states of ^{101}In and configuration-dependent shell evolution in odd-A indium isotopes, Phys. Rev. C **100**, 051303(R) (2019).

[13] Y. Xing, K. Li, Y. Zhang, X. Zhou, M. Wang, Y. Litvinov, K. Blaum, S. Wanajo, S. Kubono, G. Martinez-Pinedo *et al.*, Mass measurements of neutron-deficient Y, Zr, and Nb isotopes and their impact on rp and νp nucleosynthesis processes, Phys. Lett. B **781**, 358 (2018).

[14] M.-Z. Sun, X.-H. Zhou, W. Meng, Y.-H. Zhang, and Y. Litvinov, Precision mass measurements of short-lived nuclides at HIRFL-CSR in lanzhou, Front. Phys. **13**, 132112 (2018).

[15] Y. H. Zhang, Y. A. Litvinov, T. Uesaka, and H. S. Xu, Storage ring mass spectrometry for nuclear structure and astrophysics research, Phys. Scr. **91**, 073002 (2016).

[16] M. Hausmann, J. Stadlmann, F. Attallah, K. Beckert, P. Beller, F. Bosch, H. Eickhoff, M. Falch, B. Franczak, B. Franzke *et al.*, Isochronous mass measurements of hot exotic nuclei, Hyperfine Interact. **132**, 289 (2001).

[17] M. Hausmann, F. Attallah, K. Beckert, F. Bosch, A. Dolinskiy, H. Eickhoff, M. Falch, B. Franczak, B. Franzke, H. Geissel *et al.*, First isochronous mass spectrometry at the experimental storage ring ESR, Nucl. Instrum. Methods Phys. Res., Sect. A **446**, 569 (2000).

[18] P. Bryant, Agile, a tool for interactive lattice design, in *Proceedings of the 7th European Particle Accelerator Conference, Vienna, Austria, 2000* (EPS, Geneva, 2000), p. 1357, https://accelconf.web.cern.ch/e00/PAPERS/TUP6B03.pdf.

[19] B. Mei, X. Tu, M. Wang, H. Xu, R. Mao, Z. Hu, X. Ma, Y. Yuan, X. Zhang, P. Geng *et al.*, A high performance time-of-flight detector applied to isochronous mass measurement at CSRe, Nucl. Instrum. Methods Phys. Res., Sect. A **624**, 109 (2010).

[20] W. Zhang, X. Tu, M. Wang, Y. Zhang, H. Xu, Y. A. Litvinov, K. Blaum, R. Chen, X. Chen, C. Fu *et al.*, Time-of-flight detectors with improved timing performance for isochronous mass measurements at the CSRe, Nucl. Instrum. Methods Phys. Res., Sect. A **756**, 1 (2014).

[21] W. Zhang, X. Tu, M. Wang, Y. Zhang, H. Xu, Y. A. Litvinov, K. Blaum, X. Chen, Z. Hu, W. Huang *et al.*, A timing detector with pulsed high-voltage power supply for mass measurements at CSRe, Nucl. Instrum. Methods Phys. Res., Sect. A **755**, 38 (2014).

[22] E. J. Sternglass, Theory of secondary electron emission by high-speed ions, Phys. Rev. **108**, 1 (1957).

[23] photonis, [eb/ol], https://www.photonis.com/ (2023).

[24] J. Liu, X. Xu, P. Zhang, P. Shuai, X. Yan, Y. Zhang, M. Wang, Y. Litvinov, H. Xu, K. Blaum *et al.*, Improving the resolving power of isochronous mass spectrometry by employing an in-ring mechanical slit, Nucl. Instrum. Methods Phys. Res., Sect. B **463**, 138 (2020).

[25] Y. Xing, Y. Zhang, M. Wang, Y. Litvinov, R. Chen, X. Chen, C. Fu, H. Li, P. Shuai, M. Si *et al.*, Particle identification and revolution time corrections for the isochronous mass spectrometry in storage rings, Nucl. Instrum. Methods Phys. Res., Sect. A **941**, 162331 (2019).

[26] X. L. Tu, H. S. Xu, M. Wang, Y. H. Zhang, Y. A. Litvinov, Y. Sun, H. Schatz, X. H. Zhou, Y. J. Yuan, J. W. Xia *et al.*, Direct mass measurements of short-lived $A = 2Z - 1$ nuclides ^{63}Ge, ^{65}As, ^{67}Se, and ^{71}Kr and their impact on nucleosynthesis in the rp process, Phys. Rev. Lett. **106**, 112501 (2011).

[27] Y. H. Zhang, H. S. Xu, Y. A. Litvinov, X. L. Tu, X. L. Yan, S. Typel, K. Blaum, M. Wang, X. H. Zhou, Y. Sun *et al.*, Mass measurements of the neutron-deficient ^{41}Ti, ^{45}Cr, ^{49}Fe, and ^{53}Ni nuclides: First test of the isobaric multiplet mass equation in fp-shell nuclei, Phys. Rev. Lett. **109**, 102501 (2012).

[28] R. Chen, X. Yan, W. Ge, Y. Yuan, M. Wang, M. Sun, Y. Xing, P. Zhang, C. Fu, P. Shuai *et al.*, A method to measure the transition energy γ_t of the isochronously tuned storage ring, Nucl. Instrum. Methods Phys. Res., Sect. A **898**, 111 (2018).

[29] J. D. Scargle, Studies in astronomical time series analysis. II. Statistical aspects of spectral analysis of unevenly spaced data., Astrophys. J. **263**, 835 (1982).

[30] H. Nyquist, Certain topics in telegraph transmission theory, IEEE Trans. AIEE **47**, 617 (1928).

[31] H. Grote and F. Schmidt, Mad-x: An upgrade from mad8, in *Proceedings of the 20th Particle Accelerator Conference, PAC-2003, Portland, OR* (IEEE, New York, 2003), Vol. 5, pp. 3497–3499, https://dx.doi.org/10.1109/PAC.2003.1289960.

[32] D. A. Dahl, SIMION for the personal computer in reflection, Int. J. Mass Spectrom. **200**, 3 (2000).

[33] O. Gorda, C. Dimopoulou, A. Dolinskii, S. Litvinov, F. Nolden, and M. Steck, Field properties of the ESR magnets and their influence on beam optics—wepc058.pdf, in *Proceedings of the 2nd International Particle Accelerator Conference, IPAC 2011, San Sebastián, Spain* (EPS-AG, Spain, 2011), pp. 2148–2150, https://accelconf.web.cern.ch/IPAC2011/papers/WEPC058.PDF.

[34] W. W. Ge, Y. J. Yuan, J. C. Yang, R. J. Chen, X. L. Yan, H. Du, Z. S. Li, J. Yang, D. Y. Yin, L. J. Mao *et al.*, Experimental investigation of the transition energy $\gamma_t(B\rho)$ in the isochronous mode of the HIRFL-CSRe, Nucl. Instrum. Methods Phys. Res., Sect. A **908**, 388 (2018).

[35] K. Pearson, VII. Note on regression and inheritance in the case of two parents, Proc. R. Soc. London **58**, 240 (1895).

[36] E. Waagaard, Developing a resonance correction scheme in the LHC, Ph.D. thesis, Uppsala University, 2021, https://cds.cern.ch/record/2778017.

[37] X. L. Yan, H. S. Xu, Y. A. Litvinov, Y. H. Zhang, H. Schatz, X. L. Tu, K. Blaum, X. H. Zhou, B. H. Sun, J. J. He *et al.*, Mass measurement of ^{45}Cr and its impact on the Ca-Sc cycle in x-ray bursts, Astrophys. J. **766**, L8 (2013).

[38] P. Shuai, H. Xu, X. Tu, Y. Zhang, B. Sun, M. Wang, Y. Litvinov, K. Blaum, X. Zhou, J. He *et al.*, Charge and frequency resolved isochronous mass spectrometry and the mass of ^{51}Co, Phys. Lett. B **735**, 327 (2014).

[39] M. Wang, M. Zhang, X. Zhou, Y. H. Zhang, Y. A. Litvinov, H. S. Xu, R. J. Chen, H. Y. Deng, C. Y. Fu, W. W. Ge *et al.*, $B\rho$-defined isochronous mass spectrometry: An approach for high-precision mass measurements of short-lived nuclei, Phys. Rev. C **106**, L051301 (2022).

[40] M. Zhang, X. Zhou, M. Wang, Y. H. Zhang, Y. A. Litvinov, H. S. Xu, R. J. Chen, H. Y. Deng, C. Y. Fu, W. W. Ge *et al.*, Bρ-defined isochronous mass spectrometry and mass measurements of ^{58}Ni fragments, Eur. Phys. J. A **59**, 27 (2023).

[41] Q. Zeng, M. Wang, X. H. Zhou, Y. H. Zhang, X. L. Tu, X. C. Chen, X. Xu, Y. A. Litvinov, H. S. Xu, K. Blaum *et al.*, Half-life measurement of short-lived $^{94m}_{44}\mathbf{Ru}^{44+}$ using isochronous mass spectrometry, Phys. Rev. C **96**, 031303 (2017).

[42] K. Wille, *The Physics of Particle Accelerators: An Introduction* (Oxford University Press, Oxford, 2000), https://doi.org/10.1093/oso/9780198505501.001.0001.

[43] S. A. Litvinov, Investigation of the isochronous mode of the experimental storage ring (ESR) and the collector ring (CR). Decay spectroscopy of highly charged stored ^{140}Pr ions at the FRS-ESR facility, Ph.D. thesis, Dissertation Justus-Liebig Universität Giessen, 2008, https://www.osti.gov/etdeweb/biblio/21161773.

[44] R. J. Chen, Y. J. Yuan, M. Wang, X. Xu, P. Shuai, Y. H. Zhang, X. L. Yan, Y. M. Xing, H. S. Xu, X. H. Zhou *et al.*, Simulations of the isochronous mass spectrometry at the HIRFL-CSR, Phys. Scr. **T166**, 014044 (2015).

[45] X. Chen, M. Sanjari, P. Hülsmann, Y. Litvinov, F. Nolden, J. Piotrowski, M. Steck, T. Stöhlker, and P. Walker, Intensity-sensitive and position-resolving cavity for heavy-ion storage rings, Nucl. Instrum. Methods Phys. Res., Sect. A **826**, 39 (2016).

[46] T. Yamaguchi, H. Koura, Y. Litvinov, and M. Wang, Masses of exotic nuclei, Prog. Part. Nucl. Phys. **120**, 103882 (2021).

[47] Y. A. Litvinov and F. Bosch, Beta decay of highly charged ions, Rep. Prog. Phys. **74**, 016301 (2010).

[48] P. Walker, Y. A. Litvinov, and H. Geissel, The ILIMA project at FAIR, Int. J. Mass Spectrom. **349–350**, 247 (2013).

[49] G. Franchetti, S. Gilardoni, A. Huschauer, F. Schmidt, and R. Wasef, Space charge effects on the third order coupled resonance, Phys. Rev. Accel. Beams **20**, 081006 (2017).

[50] M. Steck and Y. A. Litvinov, Heavy-ion storage rings and their use in precision experiments with highly charged ions, Prog. Part. Nucl. Phys. **115**, 103811 (2020).